

Disorder-Driven Spin-Reorientation in Multiferroic h - $\text{YMn}_{1-x}\text{Fe}_x\text{O}_3$

Sonu Namdeo¹, S.S.S. Rao¹, S.D. Kaushik², V. Siruguri², and A.M. Awasthi^{1*}

¹*UGC-DAE-Consortium for Scientific Research, University Campus, Khandwa Road, Indore 452 001, India.*

²*UGC-DAE-Consortium for Scientific Research, Mumbai Centre, R5 Shed, Bhabha Atomic Research Centre, Mumbai 400 085, India*

ABSTRACT

Magnetic structure evolution of multiferroic hexagonal $\text{YMn}_{1-x}\text{Fe}_x\text{O}_3$ ($x= 0, 0.05,$ and 0.1) has been studied by carrying out detailed temperature-dependent neutron diffraction at zero and 5T fields. Thermodynamic data confirm antiferromagnetic ordering at T_N in all the compositions. Our sub- T_N neutron diffraction results assign the magnetic structure of pure YMnO_3 to Γ_1 irreducible representation. Over the perturbative-doping range, magnetic structure changes via $\Gamma_1+\Gamma_2$ for $\text{YMn}_{0.95}\text{Fe}_{0.05}\text{O}_3$ on to Γ_2 for $\text{YMn}_{0.9}\text{Fe}_{0.1}\text{O}_3$, as the maiden compositional analogue of spin-reorientation; its occurrence in temperature-domain already reported for several manganites. Moreover, while the large thermal isostructural changes observed above T_N are subdued in the ordered state, small alterations by the applied 5T-field are relatively uniform across, confirming strong magneto-elastic nature of the system. Decrease of the ordered magnetic moment (μ_{ord}) and planar magnetic frustration noted with Fe-doping is enhanced by the applied field; apparently through canting.

Keywords: Multiferroics, Magneto-elasticity, Frustrated Antiferromagnet, Neutron Diffraction.

PACS: 75.50.Ee, 75.85.+t, 61.05.fm, 75.75.Lf.

* Corresponding Author. E-mail: amawasthi@csr.res.in. Tel.: +91 731 2763913. Fax: +91 731 2762294.

Materials that possess coexistent magnetic and electrical orderings in single phase are known as Multiferroics.¹ Hexagonal YMnO₃ is a member of their special class known as geometrically frustrated multiferroics, and is one of the most intensively studied *h*-RMnO₃.² It undergoes ferroelectric (FE) transition at $T_C \sim 900\text{K}$ and antiferromagnetic (AFM) ordering at $T_N \sim 70\text{K}$.³⁻⁴ The crystal structure of *h*-YMnO₃ consists of alternating layers of MnO₅ trigonal bipyramids. These bipyramids (in trimer-combinations, sharing a common planar Oxygen) are corner-linked in the *ab*-plane to form a triangular lattice, and are separated from one another along the *c*-axis by the planes of Y-ions.⁵ The geometric effect of buckling of the trimerized MnO₅-bipyramids is accompanied by the inversion-symmetry-breaking displacements of Y-layers, originating the ferroelectric polarization.⁶ Regarding the magnetic structure, below T_N the Mn³⁺ moments order in the *a-b* plane, and form a 2D non-collinear spin structure, characterized by an angle of 120° between the neighbouring spins.⁷⁻⁹ Consequent to the 2D magnetism and triangular lattice, the magnetic structure of YMnO₃ is frustrated, characterized by the frustration factor $f = |\Theta_{\text{CW}}|/T_N$, found to be as large as 7.8 for YMnO₃.¹⁰ Here, Θ_{CW} is the (negative) intercept on the temperature-axis of the (interpolated) high-temperature *T*-linear (Curie-Weiss) inverse susceptibility of the independent-spins. The antiferromagnetic (AFM) order is governed by the in-plane Mn-O-Mn super-exchange interaction, whereas the Mn-O-O-Mn super-exchange interaction between the stacked triangular planes is about two order of magnitude weaker. This weak inter-layer ($z=0$ and $z=1/2$),^{4,7,11} configuration is the one that differentiates among the several magnetic structures proposed for YMnO₃, and needs to be precisely investigated. Although the magnetic structure of YMnO₃ has been studied for years, the nature of the coupling between the $z=0$ and $z=1/2$ planes is still unsettled.

According to group theory analysis, altogether six magnetic structures are found to be possible with $\mathbf{k} = 0$ vector (Goldstone modes); four 1D (Γ_1 , Γ_2 , Γ_3 , and Γ_4) and two 2D (Γ_5 and Γ_6) irreducible representations.⁷ However, all hexagonal manganites are known to particularly favour the 1D irreducible representations. Out of these four, Γ_1 and Γ_3 have antiparallel coupling of $z=0$ and $z=1/2$ moments, while Γ_2 and Γ_4 have parallel coupling. Moreover, in Γ_1 and Γ_4 representations, moments are perpendicular to the [100] axis, while in Γ_2 and Γ_3 , moments are parallel to the [100] axis. The magnetic structure of *h*-RMnO₃ was first studied in the early 1960's by the group of Bertaut and co-workers.⁴ According to them, the neutron-diffraction data of YMnO₃ can be explained by ($\Gamma_1+\Gamma_3$) representation. On the other hand, Chandrasekhar *et al.*¹² found Γ_1 representation of YMnO₃, while Munoz *et al.*⁷ and Park *et al.*⁸ found that the magnetic peaks of YMnO₃ can be explained by either Γ_1 or Γ_3 representations. Further, it was recently suggested that even pure *h*-YMnO₃ might have a mixed magnetic structure, with a mixing coefficient 0.19% of Γ_1/Γ_3 and Γ_2/Γ_4 .¹³ Furthermore, upon doping nonmagnetic atoms (c.f., Al, Ru, and Zn) only up to 10% at the Mn-site, mixing of the two representations gets increased.¹⁴ Therefore, the magnetic structure of YMnO₃ remains somewhat uncertain.

Recently, Sharma *et al.*¹⁵ carried out a comparative study by Ti⁴⁺ (d^0), Fe³⁺ (d^5), and Ga³⁺ (d^{10}) (only 10%) doping at the Mn-site. Below $T_N \sim 75\text{K}$, the magnetic structure of YMnO₃ was described as a linear combination of irreducible representations Γ_3 and Γ_4 , the ratio of which changed with lowering the temperature. The change of magnetic structure to Γ_2 was caused by Ti, and with Fe-doping, the magnetic structure was described by the irreducible representation Γ_3 , which below 35K underwent spin-reorientation to Γ_3 plus 51% Γ_4 . On the other hand, rare-earth (Er) doping at Y-site¹² resulted in the change of magnetic ground state from Γ_1 to Γ_2 , and also induced spin-reorientation transition via intermediate ($\Gamma_1+\Gamma_2$) configuration for half-doped Y_{0.5}Er_{0.5}MnO₃. Kozlenko *et al.*¹⁶ in their pressure-dependent neutron diffraction study on YMnO₃ showed that on application of up to 6GPa external pressure, pure YMnO₃ also undergoes spin-reorientation transition, analogous to temperature domain (T_{sr})^{7,17} in ScMnO₃ and HoMnO₃. Lee *et al.*¹⁸ found via high-resolution neutron diffraction that all structural parameters abruptly change at T_N ; evidencing strong and direct spin-lattice coupling. Moreover, recently giant magneto-elastic (MEL) coupling has been observed in YMnO₃,¹⁹⁻²⁰ and the dominance of this MEL over a weaker magneto-electric (ME) coupling in the coexistent FE and AFM phases of YMnO₃ has been reported by field-dependent neutron diffraction experiments.²¹ The effects of magnetic doping on the magnetic structure of YMnO₃ have rarely been investigated. Therefore, perturbed by the magnetic Fe-ion at the Mn-site, we have explored the modification of the magnetic structure of YMnO₃. This study provides valuable new insights to correlate the changes of magnetic structure with the properties.

Polycrystalline samples of YMn_{1-x}Fe_xO₃ ($x = 0, 0.05, \text{ and } 0.1$) were synthesized by conventional solid state reaction route. Stoichiometric amounts of high purity ($> 99.99\%$) Y₂O₃, MnO₂, and Fe₂O₃ powders were thoroughly mixed and calcined at 1200°C for 27 hrs. The resultant powders were pelletized and sintered in air at 1400°C for a total of 27 hrs, along with intermediate grinding. XRD of the prepared samples were obtained by Bruker D8 X-ray diffractometer, with Cu-K α radiation ($\lambda=1.54\text{\AA}$). Magnetization and specific heat data were taken using a Quantum Design 14T MPMS-Vibrating sample magnetometer (VSM) and PPMS, respectively. The neutron diffraction (ND) measurements were carried out at wavelength of 1.48Å on powder samples, using the multi-position-sensitive-detector-based focusing crystal diffractometer, set up by UGC-DAE CSR (Mumbai Centre), at the National Facility for Neutron Beam Research (NFNBR), Dhruva reactor, Mumbai (India). ND patterns were collected at 10K, 30K, 50K, 60K, 70K, 100K, 200K, and 300K. The samples were placed in Vanadium-can, which was directly exposed to the neutron beam at 300K, while for low-temperature measurements, Vanadium-can filled with powder samples was loaded in a Cryogenic-make cryogen-free magnet system. ND data were taken in the warming cycle and were Rietveld-refined for both crystalline and magnetic parts, using FULLPROF program.²²

The as-prepared samples were first subjected to XRD measurements for its structural characterization. All the XRD patterns were indexed to hexagonal structure with space group $P6_3cm$. Figure 1 shows the specific heat in the temperature range from 2-200K under zero and 5T magnetic fields. The C_p -data show a prominent peak, confirming the AFM ordering temperature which well-correlates with our magnetization data, discussed below. The absence of any secondary peak around 43K in the data confirms that as-prepared samples do not contain any impurity phase (e.g., ferrimagnetic Mn_3O_4).²³ Also, the T -position of this peak is unaffected up to 5T magnetic field. As the well-known feature of these hexagonal manganites, signature of magnetic frustration in the C_p - T data have been reported²⁴ as large magnetic-entropy reductions above T_N .

Before performing neutron diffraction (ND), we measured DC magnetization from 10 to 300K, in an applied field of 100 Oe under ZFC and FC conditions. All the specimens exhibit very weak antiferromagnetic (AFM) transition as small kinks at T_N , shown in $1/\chi = H/M$ vs. T plots (fig.2, left panels). For robust AFM ordering (no magnetic-frustration), spin-correlations above the transition temperature are absent, and the high-temperature linear Curie-Weiss behaviour ($1/\chi \sim [T - \Theta_{CW}]$) of independent (i.e., uncorrelated) spins continues down to T_N . In such cases, magnitude of the Curie-Weiss temperature $|\Theta_{CW}|$ exactly matches with that of the ordering temperature T_N (frustration-parameter $f = |\Theta_{CW}|/T_N \equiv 1$). By the same token, any deviation (above T_N) from the high- T linear-behaviour is taken as indication of magnetic frustration, concurrent with $f > 1$.²⁵⁻²⁶ Magnetic frustration is evident in the present $1/\chi$ - T data as well; deviating from the Curie-Weiss linear-fit at $T \geq 150K > T_N$. The interpolated linear fits over 150-300K to the $(1/\chi$ - $T)$ plot intercept on the (-ve) temperature axis, providing the value of Curie-Weiss temperature (Θ_{CW}) and the fit's-slope provides effective magnetic moment (μ_{eff}). The value of Θ_{CW} (estimated error $\pm 5K$) is found to decrease from $\Theta_{CW} = -533.59K$ for $YMnO_3$ to $-463.88K$ for $YMn_{0.95}Fe_{0.05}O_3$, and to $-426.75K$ for $YMn_{0.90}Fe_{0.10}O_3$. Since Θ_{CW} is a measure of the AFM coupling strength between the Mn-ions, the results suggest that Fe-doping suppresses the Mn-O-Mn AFM superexchange. Simultaneously, the estimated effective magnetic moment (estimated error $\pm 0.05\mu_B$) also shows a similar change: $\mu_{eff} = 5.45\mu_B$ estimated for $YMnO_3$ reduces to $5.27\mu_B$ for $YMn_{0.95}Fe_{0.05}O_3$ and to $5.04\mu_B$ for $YMn_{0.9}Fe_{0.1}O_3$. As Fe^{+3} has higher magnetic moment ($5.92\mu_B$) compared to that of Mn^{+3} ($4.90\mu_B$), the observed decreasing trend of effective magnetic moment rules out that Fe-ions are in the Fe^{+3} state, which is consistent with a previous report by some of us.²⁷ In addition, the frustration parameter $f = |\Theta_{CW}|/T_N$ decreases with Fe-doping from 7.51 for $YMnO_3$ to 6.53 for $YMn_{0.95}Fe_{0.05}O_3$, on to 6.10 for $YMn_{0.9}Fe_{0.1}O_3$. This trend of magnetic parameters is consistent with our previous work,²⁷ though the improved accuracy has resulted due to the increased sintering time of the fresh samples prepared, with density of the pellets increased and the possibility of oxygen vacancies reduced.

The AFM transition is more obvious in the differentiated dM/dT curves, shown in field-cooled (FC) and zero-field-cooled (ZFC) cycles (right-panels, bottom/left axes). The transition temperatures T_N (VSM precision $\pm 10\text{mK}$) obtained from the discontinuity in the slope is found to be 71K for YMnO_3 , 71K for $\text{YMn}_{0.95}\text{Fe}_{0.05}\text{O}_3$, and 70K for $\text{YMn}_{0.9}\text{Fe}_{0.1}\text{O}_3$. Also shown (right-panels, top/right axes) is the relative difference $(M_{FC}/M_{ZFC}-1)$ between the field-cooled warming (FCW) and zero-field cooled warming (ZFCW) data. This signifies weak ferromagnetism (WFM) evolution below T_N ,^{25,28} since the (otherwise fluctuating) field-aligned (FC) spins are increasingly stabilized in the ordered state. Due to higher magnetic frustration (f) implying larger AFM-correlations above T_N in pure YMnO_3 , the spontaneous internal field at T_N is less robust,²⁹ reflected as less-prominent anomalies in both $1/\chi-T$ and dM/dT at its AFM-transition. Therefore, regarding the ability to field-align the fluctuating-spins across T_N in an FC-protocol, external field reckons relatively stronger in pure versus the doped specimens, resulting in an observable FC-ZFC hysteresis near T_N in the former. In contrast, Fe-doped specimens show large FC-ZFC hysteresis at *low temperatures*, versus a much-smaller one in the pure YMnO_3 . Due to magnetic disorder, Fe-doped samples feature smaller saturation ordered moments (μ_{ords} , obtained from the ND data and shown later in fig.8) vis-à-vis the pure YMnO_3 . The *non* AFM-ordering Fe- and the *less* AFM-ordered Mn- spins (in the Γ_1 and/or Γ_2 domains; short-range FM Fe-O-Mn interactions²⁵ competing with long-range AFM Mn-O-Mn one), and the weakly-ordered spins residing in the Γ_1 - Γ_2 domain-walls (as explained later), are all susceptible to field-align in an FC protocol, at low-temperatures. This may explain the large (smaller) low- T FC-ZFC hysteresis in the doped (pure) specimens. Note the higher saturation-value of the relative difference $(M_{FC}/M_{ZFC}-1)$ for 5% Fe-doping, compared to both the pure and 10% Fe-doped compositions; later traced to the inhomogeneous magnetic structure of $\text{YMn}_{0.95}\text{Fe}_{0.05}\text{O}_3$.

Figure 3 shows the Rietveld-refined ND patterns of $\text{YMn}_{1-x}\text{Fe}_x\text{O}_3$ ($x=0, 0.05, \text{ and } 0.1$) at 300K and 10K. The absence of any unaccounted peak in the refined data confirms the single-phasic nature of the specimens. Now, in order to determine the magnetic structure of our specimens, zero-field neutron diffraction data collected at 10K were used. Figure 4 shows the observed intensity-plots over a zoomed-in 2Θ -range at 10K for all three specimens. It is obvious from the low-temperature ND pattern that with Fe-doping at the Mn-site, the weightage of the prominent magnetic peak (100) at $2\Theta \sim 16.04^\circ$ in the pure YMnO_3 gets systematically transferred to the (101) peak at $2\Theta \sim 17.67^\circ$. Also, the intensity of the purely magnetic (100) Bragg peak is found to decrease in $\text{YMn}_{0.95}\text{Fe}_{0.05}\text{O}_3$, while it completely disappears in $\text{YMn}_{0.9}\text{Fe}_{0.1}\text{O}_3$. Additionally, thermal evolutions of (100) and (101) peaks shown in figure 5 clearly evidence their intensity ratio $I_{(100)}/I_{(101)}$ varying with the Fe-content. These observations correspond to the change with Fe-doping, of Mn's ordered-magnetic-moment, and its orientation in the a - b plane. Raw-data manifestation of the magnetic structure modification vs. nominal doping is further confirmed by the magnetic phase analysis as follows.

Intensity of the magnetic peaks increases to constant values at 10K, suggesting that the magnetic structures have stabilized by the lowest temperature covered. In the attempt to fit the data, all 1D irreducible representation vectors Γ_1 , Γ_2 , Γ_3 , and Γ_4 were generated for propagation vector $\mathbf{k} = 0$, by using BasIreps program in FULLPROF suite.²² Figure 6 shows the Rietveld-refined neutron diffraction patterns at 10K without field (for all compositions) and under 5T-field (for the doped specimens). The data across $2\theta \sim 60^\circ$, due to the contribution of peaks from the shroud of the cryogen-free magnet, was excluded in the refinement process. Now, firstly considering the case of YMnO_3 , we had tried to fit the data with various possible magnetic models proposed in the literature (as discussed in the introduction). The best fit though was obtained for the magnetic structure given by the basis vectors of the irreducible representation Γ_1 (fig.6(a)), consistent with the previous reports.^{7,12,21} Moreover, the neutron diffraction data of $\text{YMn}_{0.95}\text{Fe}_{0.05}\text{O}_3$ was best fit with the admixture ($\Gamma_1 + \Gamma_2$) of irreducible representations (fig. 6(b), (c)). Lastly, the Γ_2 representation was best fit for $\text{YMn}_{0.9}\text{Fe}_{0.1}\text{O}_3$ (figs. 6(d), (e)).

The change of magnetic structure on Fe-doping is but compositional analogue of the changes observed across the spin-reorientation temperature (T_{sr}) in e.g., ScMnO_3 and HoMnO_3 ,^{7,17} and in YMnO_3 under pressure.¹⁶ Therefore, here we maidenly witness the chemically-driven spin-reorientation by perturbative Fe-doping in YMnO_3 . The mixed ($\Gamma_1 + \Gamma_2$) configuration reflects inhomogeneous magnetic structure for the 5% Fe-doped $\text{YMn}_{0.95}\text{Fe}_{0.05}\text{O}_3$, with the possibility of statistically-distributed Γ_1 and Γ_2 ‘domains’. Their interfacial “domain-walls spins” would exhibit higher propensity to harbour weak ferromagnetism (WFM), much the same way as found by breaking the long-range cycloidal-AFM order in BiFeO_3 .³⁰ As seen earlier in our bulk magnetization results, this circumstance is in fact consistent with the higher saturation value of the relative change ($M_{FC}/M_{ZFC} - 1$) for the mixed-configuration $\text{YMn}_{0.95}\text{Fe}_{0.05}\text{O}_3$, compared to the same for both the pure YMnO_3 (Γ_1) and $\text{YMn}_{0.9}\text{Fe}_{0.1}\text{O}_3$ (Γ_2) uniform magnetic structures. WFM may arise from fluctuating local-spins²⁹ that either (a) do not order antiferromagnetically (e.g., the Fe-spins in the present doped-specimens, or (b) are not robustly aligned at the transition temperature (due to a weaker spontaneous magnetization, traceable to spin-correlations in the disordered state), or (c) remain uncompensated at low-temperatures, due to the breakage of uniform magnetic structure by impurity (e.g., doping-induced disruption of the long-range cycloidal magnetic-order in BiFeO_3 ,³⁰ or of the triangular Mn-spins’ arrangement by Fe in the present case), or (d) inhabit the ‘interfacial’ regions (weakly-ordered/uncompensated) between existing differently AFM-ordered ‘domains’ (such as Γ_1 and Γ_2 in the present $\text{YMn}_{0.95}\text{Fe}_{0.05}\text{O}_3$ specimen). This, as well as canting (absence of the exact cancellation of skewed-AFM-ordered moments³¹) produced either by an applied field (in the present case of ND at 5T), material-anisotropy, or short-range FM (viz., inverse D-M interaction)^{25,28} all provide sources of weak ferromagnetism (WFM); producing split of the FC-ZFC magnetizations and manifesting as

field-dependent reduced ordered-moments (μ_{ord} , determined as ‘AFM-aligned-projection’ of the field-skewed moment).

Singh *et al.*²¹ have shown that the ND data of pure YMnO₃ under an applied field of 5T field could be refined by using the same Γ_1 irreducible representation. Therefore, to further examine we have investigated the field-effect on the doped specimens only, by carrying out their neutron diffraction under 5T field. For this, after collecting the data at each temperature, field was reduced to zero and sample temperature was raised well beyond the Néel temperature, to erase the possibility of frozen field-aligned spins. Figs. 6(c) & (e) show the Rietveld-refined in-field neutron diffraction patterns at 10K for YMn_{0.95}Fe_{0.05}O₃ and YMn_{0.9}Fe_{0.1}O₃ respectively. It is found that the ND data taken under 5T field could be refined by using the same irreducible representations as assigned for the zero-field data; ($\Gamma_1+\Gamma_2$) for YMn_{0.95}Fe_{0.05}O₃ and Γ_2 for YMn_{0.9}Fe_{0.1}O₃.

Figure7 (left panel) show temperature dependence of the lattice parameters a and c for YMnO₃, YMn_{0.95}Fe_{0.05}O₃, and YMn_{0.9}Fe_{0.1}O₃, with the field-induced alteration shown only for doped specimens, as obtained by the Rietveld refinement. The refined lattice parameters (under zero-field) match well with the previous reports.^{9,18-19} The lattice parameter a (c) shows the positive (negative) thermal expansion. Thermal contraction of the lattice parameter c is reported to be persistent up to the ferroelectric transition.^{9,32} Both a and c show large changes above T_N , and the applied field further alters the values of all the lattice parameters. In particular, note the *magneto-expansion* of c lattice constant for the doped-specimens here, as opposed to its *magneto-contraction* reported²¹ for the pure specimen. Positive magneto-expansion of c reflects increased tilting (buckling) of MnO₅ polyhedra (Y-O planes), indicating enhanced ferroelectric polarization P under the field, as against latter’s decrease with *thermal contraction* of c , restoring the inversion-symmetry. The bond-lengths under zero and 5T field at 10K are summarized in TABLE I. Alteration of these bonds with the applied field confirms the presence of strong magneto-elastic (MEL) coupling in the doped specimens as well, though their observed trend here is different from those reported²¹ for the pure YMnO₃. Figure 7 (right panel) shows the temperature-evolution and field-alteration of the planar bond-length (Mn-O_p, average of one Mn-O(3) and two Mn-O(4) equatorial bond-lengths), which governs the magnetic ordering, and is found to increase with temperature for all three compositions and also with field for the doped-specimens. Also, the slight increase in the planar bond-length with the Fe-content indicates the weakening of the superexchange interaction due to the dilution of Mn-ions and therefore, suppresses T_N minutely. These results well correlate with our magnetization and specific heat data.

Figure 8 shows the T -dependence for pure & doped specimens and H -alteration for the latter, of the ordered magnetic moment (μ_{ord}) at the Mn-site, explicitly obtained by the Rietveld refinement of our neutron diffraction data. Below T_N , μ_{ord} increases for all three compositions and reaches their respective saturation values. For pure YMnO₃, the saturation μ_{ord} is estimated as $3.41\mu_B$; smaller than the ionic value of $4.0\mu_B$ for Mn⁺³. Therefore, about $0.6\mu_B$ (15%) of the Mn-moment is still fluctuating

at 10K in YMnO₃. This difference is the microscopic evidence of 2D geometrical frustration of the Mn-lattice. The saturation-value is 3.16μ_B for YMn_{0.95}Fe_{0.05}O₃ and 3.08μ_B for YMn_{0.9}Fe_{0.1}O₃; interestingly, the ratio 3.08/3.41 = 0.903 of μ_{ord}(10K) for 10% Fe-doped and pure (undoped) specimens reflects but the compositional ratio (1-x) of their Mn-contents, as also confirmed (shown below) up to 60K. This precise scaling leads to an important insight that the chemo-magnetically disordered Fe-dopant's moment is *fully-fluctuating* and thus non-contributing to the measured ordered-moment. The nearly parallel lines drawn at T < T_N in Fig.8-inset, connecting the [scaled by μ_{ord}(10K, x=0)] zero-field ordered-moments of the two pure (Γ₁/YMnO₃ and Γ₂/YMn_{0.9}Fe_{0.1}O₃) structures illustrate the indifference (to Γ₁ or Γ₂) of individual Mn's ordered-moment part; solely contributing below T_N to μ_{ord}(T), in proportion to their Mn-population alone. Moreover, clearly discernible *below-the-line* values of the scaled-μ_{ord}(T) for the mixed [(Γ₁+Γ₂)/YMn_{0.95}Fe_{0.05}O₃] configuration reflect enhanced Mn-moments' fluctuation at 10K (≈ 17% here vs. ~15% in YMnO₃).

Under 5T field, saturation-μ_{ord} reduces further; to 95% for YMn_{0.95}Fe_{0.05}O₃ and to 98% for YMn_{0.9}Fe_{0.1}O₃, of their respective zero-field values. Considering the applied field to cause off-plane canting (skewing) of the Mn-moments (as the ND-estimated ordered-moment is but its average planar component, partaking in triangular AFM-formation), the (vertical) canting-angle would therefore satisfy cos ψ = μ_{ord}(5T)/μ_{ord}(0T). Angles ψ thus evaluated at 10K/70K is ≈10.58°/19.36° for YMn_{0.95}Fe_{0.05}O₃ and ≈10.13°/28.56° for YMn_{0.9}Fe_{0.1}O₃. Evidently, the more frustrated specimen exhibits less susceptibility to canting near T_N, albeit being almost equally susceptible at low T's. Anti-regression of the *maximum* (70K) vertical-canting and planar-frustration of the moments is beautifully underscored by the excellent equality of the ratio [cos ψ_{5%Fe}/cos ψ_{10%Fe}]_{70K} = 1.074 of moment's canting-direction-cosines, and that of the bulk frustrations f_{5%Fe}/f_{10%Fe} = 1.072, for YMn_{0.95}Fe_{0.05}O₃ and YMn_{0.9}Fe_{0.1}O₃ specimens. Moreover, at low-T's we similarly note that the compositional-ratio of the (5T) field-induced canted-WFM moments (C-WFM) [(μ_{ord}sin ψ)_{5%Fe}/(μ_{ord}sin ψ)_{10%Fe}]_{10K} = 1.072 agrees (to ≤ 10%) with that of the measures of their saturation weak ferromagnetism (S-WFM), definable as [(M_{FC}/M_{ZFC}-1)_{5%Fe}/(M_{FC}/M_{ZFC}-1)_{10%Fe}]_{10K} = 1.176. The larger difference here being due to the direct origin (post ZFC, 5T-field in the AFM state) of the former and the quenched-canted origin (post FC, 100 Oe field in the PM state) of the latter ratio.

To further examine the more interesting *physically-mixed* YMn_{0.95}Fe_{0.05}O₃ composition, *mathematical* Φ(T) evaluated as the 'statistical-average' of the (zero-field) angle between the Mn-moment and the a-axis (90° for Γ₁ and 0° for Γ₂ configuration^{7,12}) is shown in fig.9 (left y-axis). This lies between 77.98° (10K) to 3.56° (70K); providing the base-data for thermal evolution of the mixed (Γ₁+Γ₂) magnetic structure in YMn_{0.95}Fe_{0.05}O₃. Now, the relative abundance p₁ (p₂=1-p₁) of Γ₁ (Γ₂) configuration satisfy Φ = 90p₁+0p₂, so that p₁= Φ/90 and p₂=1-Φ/90. Moreover, referred to fig.8-inset, for this specimen the (ideal) *fully-ordered-moment* per Mn-site ought to satisfy

$\mu_{ord}^{full}(x = 0.05)/\mu(\text{Mn}^{+3}) \approx 95\%$, with the ionic $\mu(\text{Mn}^{+3}) = 4.0\mu_B$, whilst its (practical) *maximally*-ordered-moment is expected as $\mu_{ord}^{max}(T, x = 0.05) \approx 0.95\mu_{ord}(T, x=0)$ at finite T 's. The low- T -dominant Γ_1 -share ($= p_1[\mu_{ord}(T, x=0.05)/\mu_{ord}^{full}(x = 0.05)]_{0T}$) is seen in fig.9 (right y -axis) to drop from 72% (10K) through 10% (60K) to 1.6% (70K), whereas the Γ_2 -fraction ($= p_2[\mu_{ord}(T, x=0.05)/\mu_{ord}^{full}(x = 0.05)]_{0T}$) rises from 11% (10K) through (max.) 52% (60K) up to 39% (70K) near T_N . The shortage of these fractions' sum below unity ($1-[\mu_{ord}(T, x=0.05)/\mu_{ord}^{full}(x = 0.05)]_{0T}$) represents the gross-fraction of residual-fluctuating Mn-spins; its temperature-evolution ($\sim 17\%$ at 10K to $\sim 59\%$ at 70K) shown in fig.9-inset (left y -axis). Furthermore, estimated net-fraction of weakly-ordered Mn-spins in the interfacial Γ_1 - Γ_2 domain-walls ($1-[\mu_{ord}(T, x=0.05)/\mu_{ord}^{max}(T, x = 0.05)]_{0T}$) reduces from (max.) 2.2% at 10K (fig.9-inset, right y -axis). These results are consistent with our μ_{ord} and Φ -angle analyses.

CONCLUSIONS

In summary, we have carried out neutron diffraction study of perturbatively (up to 10%) Fe-doped polycrystalline h -YMn $_{1-x}$ Fe $_x$ O $_3$ below and above the Néel temperature in zero- (all specimens) and under 5T-field (doped compositions). The lattice parameters and planar bond-lengths show large (minute) changes above (below) T_N , nearly uniformly altered (in the doped specimens) by the 5T field across the AFM and PM states, exhibiting strong magneto-elastic nature of the system. Our study highlights spin re-orientation in the hexagonal manganite, composition-driven by the magnetic (Fe) doping; the magnetic ground state changes from a highly-frustrated (Γ_1 /YMnO $_3$) to a lowly-frustrated (Γ_2 /YMn $_{0.9}$ Fe $_{0.1}$ O $_3$) magnetic structure, via a mixed [$(\Gamma_1+\Gamma_2)$ /YMn $_{0.95}$ Fe $_{0.05}$ O $_3$] configuration, which thermally evolves from Γ_1 -rich (low- T) to Γ_2 -rich (near- T_N) character. The applied 5T field does not qualitatively alter the overall magnetic structures of the doped specimens; it adds to the disorder-induced suppression of the evaluated/planar-component of the ordered moment (μ_{ord}) via latter's off-plane/vertical canting. Therefore, magnetic field enhances the doping-induced relief of the planar magnetic frustration. Concerning geometric multiferroicity of the system, a qualitative change in its magneto-electric coupling hand-in-hand with disorder-driven spin-reorientation emerges from the present study. This important implication is compelled by the observed magneto-expansion of the c lattice constant (signifying⁹ +ve magneto-polarisation dP/dH) in the doped specimens, vis-à-vis literature-reported²¹ magneto-compression of c (i.e., -ve dP/dH) in pure YMnO $_3$.

ACKNOWLEDGEMENTS

We thank Mukul Gupta, V. Ganesan, and A. Banerjee for providing XRD, specific heat, and magnetization facilities respectively, and D. Kumar for help with the magnetization measurements. P. Chaddah is acknowledged for his scientific support and encouragement.

REFERENCES

- ¹N. Hur, S. Park, P. A. Sharma, J.S. Ahn, S. Guha, and S.-W. Cheong, *Nature (London)* **429**, 392 (2004).
- ²N.A. Spaldin and M. Fiebig, *Science* **309**, 391 (2005); S.-W. Cheong, and M. Mostovoy, *Nature Mater.* **6**, 13 (2007).
- ³I.G. Ismailzade, and S.A. Kizhaev, *Sov. Phys. Solid State* **7**, 236 (1965).
- ⁴E.F. Bertaut and M. Mercier, *Phys. Lett.* **5**, 27 (1963); E.F. Bertaut, R. Pauthenet, and M. Mercier, *Phys. Lett.* **7**, 110 (1963); W.C. Koehler, L. Yakel, E.O. Wollen, and J.W. Cable, *Phys. Lett.* **9**, 93 (1964).
- ⁵H. Yakel, W.C. Koehler, E.F. Bertaut, and F. Forrat, *Acta Crystallogr.* **16**, 957 (1963).
- ⁶B.B. Van Aken, T.T.M. Palstra, A. Filippetti, and N.A. Spaldin, *Nature Mater.* **3**, 164 (2004); C.J. Fennie and K.M. Rabe, *Phys. Rev. B* **72**, 100103(R) (2005).
- ⁷A. Munoz, J.A. Alonso, M.J. Martinez-Lope, M.T. Casais, J.L. Martinez, and M.T. Fernandez-Diaz, *Phys. Rev. B* **62**, 9498 (2000).
- ⁸J. Park, U. Kong, S.I. Choi, J.-G. Park, C. Lee, and W. Jo., *Appl. Phys. A: Mater. Sci. Process.* **A74**, S796 (2002).
- ⁹T. Katsufuji, M. Masaki, A. Machida, K. Kato, E. Nishibori, M. Takata, M. Sakata, K. Ohoyama, K. Kitazawa, and H. Takagi, *Phys. Rev. B* **66**, 134434 (2002).
- ¹⁰A.P. Ramirez, in *Handbook of Magnetic Materials*, edited by K.H.J. Buschow (North-Holland, Amsterdam, 2001), Vol. **13**.
- ¹¹T.J. Sato, S.-H. Lee, T. Katsufujii, M. Masaki, S. Park, J.R.D. Copley, and H. Takagi, *Phys. Rev. B* **68**, 014432(2003).
- ¹²M.C. Sekhar, S. Lee, G. Choi, C. Lee, and J.-G. Park, *Phys. Rev. B* **72**, 014402 (2005).
- ¹³P.J. Brown and T. Chatterji, *J. Phys.: Condens. Matter* **18**, 10085 (2006).
- ¹⁴J. Park, M. Kang, J. 23, S. Lee, K.-H. Jang, A. Pirogov, J.-G. Park, C. Lee, S.-H. Park, and H.C. 23, *Phys. Rev. B* **79**, 064417 (2009).
- ¹⁵N. Sharma, A. Das, C.L. Prajapat, and S.S. Meena, *J. Magn. Magn. Mater.* **348**, 120 (2013).
- ¹⁶D.P. Kozlenko, S.E. Kichanov, S. Lee, J.-G. Park, and B.N. Savenko, *J. Phys.: Condens. Matter* **19**, 156228 (2007).
- ¹⁷M. Fiebig, D. Frohlich, K. Kohn, St. Leute, Th. Lottermoser, V.V. Pavlon, and R.V. Pisarev, *Phys. Rev. Lett.* **84**, 5620 (2000); A. Munoz, J.A. Alonso, M.J. Martinez-Lope, M.T. Casais, J.L. Martinez, and M.T. Fernandez-Dias, *Chem. Mater.* **13**, 1497 (2001); Th. Lonkal, D. Hohlwein, J. Ihringer, and W. Prandal, *Appl. Phys. A* **74**, S843 (2002); O.P. Vajk, M. Kenzelmann, J.W. Lynn, S.B. 23, and S.-W. Cheong, *Phys. Rev. Lett.* **94**, 087601 (2005).
- ¹⁸S. Lee, A. Pirogov, J.H. Han, J.-G. Park, A. Hoshikawa, and T. Kamiyama., *Phys. Rev. B* **71**, 180413R (2005).
- ¹⁹S. Lee, A. Pirogov, M. Kang, K.-H. Jang, M. Yonemura, T. Ka-miyama, S.-W. Cheong, F. Gozzo, N. Shin, H. 23ura, Y. Noda, and J.-G. Park, *Nature Mater.* **451**, 805 (2008).
- ²⁰T. Chatterji, B. Ouladdiaf, P.F. Henry, and D. Bhattacharya, *J. Phys.: Condens. Matter* **27**, 336003 (2012).

- ²¹A.K. Singh, S. Patnaik, S.D. Kaushik, and V. Siruguri, Phys. Rev. B **81**, 184406 (2010).
- ²²J. Rodriguez-Carvajal, Physica B **192**, 55 (1993).
- ²³M. 23, X.M. Chen, Y.I. Joe, E. Fradkin, P. Abbamonte, and S.L. Cooper, Phys. Rev. Lett. **104**, 136402 (2010).
- ²⁴D.G. Tomuta, S. Ramakrishnan, G.J. Nieuwenhuys and J.A. Mydosh, J. Phys.: Condens. Matter **13**, 4543 (2001).
- ²⁵M. Zaghrioui, J.M. Grene `che, C. Autret-Lambert, and M. Gervais, J. Magn. Magn. Mater. **323**, 509 (2011).
- ²⁶Chen et al., J. Phys.: Condens. Matter **17**, 8029 (2005).
- ²⁷S. Namdeo, A.K. Sinha, M.N. Singh, and A.M. Awasthi, J. Appl. Phys. **113**, 104101 (2013).
- ²⁸Y.J. Yoo, Y.P. Lee, J.S. Park, J.-H. Kang, J. 23, B.W. Lee, and M.S. Seo, J. Appl. Phys. **112**, 013903 (2012).
- ²⁹Chao Zhang *et al.*; J. Alloys. Compounds **509**, 7738 (2011).
- ³⁰I. Sosnowska, W. Schäfer, W. Kockelmann, K.H. Andersen, and I.O. Troyanchuk, Appl. Phys. A: Mater. Sci. Process. **74**, S1040 (2002); G. Catalan, K. Sardar, N.S. Church, J.F. Scott, R.J. Harrison, and S.A.T. Redfern, Phys. Rev. B **79**, 212715 (2009).
- ³¹Joy et al., J. Phys.: Condens. Matter **10**, 11049 (1998).
- ³²Il-Kyoung Jeong, N. Hur, and Th. Proffenc, J. Appl. Cryst. **40**, 730 (2007); A.S. Gibbs, K.S. Knight, and P. Lightfoot, Phys. Rev. B **83**, 094111 (2011).

Table Captions

Table-I. Mn-O [O(1), O(2), O(3), and O(4)] bond-lengths and Mn--Mn distance at 10K for YMnO₃ (0T), YMn_{0.95}Fe_{0.05}O₃ (0T, 5T), and YMn_{0.9}Fe_{0.1}O₃ (0T, 5T).

TABLE I

Specimen	YMnO ₃ (0T)	YMn _{0.95} Fe _{0.05} O ₃ (0T)	YMn _{0.95} Fe _{0.05} O ₃ (5T)	YMn _{0.9} Fe _{0.1} O ₃ (0T)	YMn _{0.9} Fe _{0.1} O ₃ (5T)
Bond- Length (Å)					
Mn-O(1)	1.75491(8)	1.75771(9)	1.75756(9)	1.75792(8)	1.75840(9)
Mn-O(2)	1.97229(9)	1.97542(10)	1.97525(10)	1.97566(9)	1.97620(10)
Mn-O(3)	2.00750(5)	2.00859(10)	2.00904(6)	2.00904(5)	2.00930(5)
Mn-O(4)	2.07165(4)	2.07274(7)	2.07322(5)	2.07321(4)	2.07348(4)
Mn--Mn	3.57985(10)	3.58217(9)	3.58254(10)	3.58272(9)	3.58286(8)

Figure Captions

Fig.1. The temperature dependence of C_p/T for $\text{YMn}_{1-x}\text{Fe}_x\text{O}_3$ ($x= 0, 0.05,$ and 0.1) under zero- and 5T-fields. Open (filled) symbols show the data points in zero (5T) field.

Fig.2. Left panels: inverse-susceptibility ($1/\chi = H/M$) vs. temperature plot for $\text{YMn}_{1-x}\text{Fe}_x\text{O}_3$ ($x= 0, 0.05,$ and 0.1). Straight lines (fitted over 150-300K data) correspond to the Curie-Weiss law. Right panels: FC-ZFC magnetization hysteresis, clearly manifested in the derivatives dM/dT (bottom/left axes) and the relative change between the FCW/ZFCW data (top/right axes), as a quantitative measure of the weak ferromagnetism (WFM) evolution in the ordered AFM state, with different prominence-regimes in pure (around T_N) and doped (low- T 's) specimens, and its predominance in the mixed ($\Gamma_1+\Gamma_2$) magnetic-structured $\text{YMn}_{0.95}\text{Fe}_{0.05}\text{O}_3$.

Fig.3. (a), (c), & (e)-- Rietveld-refined neutron diffraction pattern for $\text{YMn}_{1-x}\text{Fe}_x\text{O}_3$ ($x= 0, 0.05,$ and 0.1), taken at 300K. (b), (d), & (f)-- Rietveld-refined neutron diffraction pattern for $\text{YMn}_{1-x}\text{Fe}_x\text{O}_3$ ($x= 0, 0.05,$ and 0.1) taken at 10K under zero field.

Fig.4. Bragg-peak pattern over zoomed-in 2Θ -range for $\text{YMn}_{1-x}\text{Fe}_x\text{O}_3$ ($x= 0, 0.05,$ and 0.1), taken at 10K under zero field. The data are shifted upwards for clarity. Inset shows the survey pattern for YMnO_3 .

Fig.5. Intensity vs. temperature plot of (100) & (101) magnetic peaks at zero field for $\text{YMn}_{1-x}\text{Fe}_x\text{O}_3$ ($x= 0, 0.05,$ and 0.1).

Fig.6. Observed (10K) and calculated neutron diffraction patterns with $P6_3cm$ symmetry for $\text{YMn}_{1-x}\text{Fe}_x\text{O}_3$ ($x= 0, 0.05,$ and 0.1). To refine the data, we used (a) Γ_1 representation for YMnO_3 , (b) & (c) ($\Gamma_1+\Gamma_2$) representation for $\text{YMn}_{0.95}\text{Fe}_{0.05}\text{O}_3$ under zero- and 5T-fields respectively, and (d) & (e) Γ_2 -representation for $\text{YMn}_{0.9}\text{Fe}_{0.1}\text{O}_3$ under zero- and 5T-fields, respectively. Lines below the bars indicate the difference between the observed and calculated neutron diffraction patterns. Upper and lower bars correspond respectively to nuclear and magnetic Bragg peaks.

Fig.7. Left panels: temperature-dependence of the lattice parameters a and c for $\text{YMn}_{1-x}\text{Fe}_x\text{O}_3$ (all compositions) and their alteration under 5T-field (doped-specimens). Right panels: average planar (Mn-O_p) bond-length evaluated by using Mn-O(3) & Mn-O(4) bond-lengths under zero-field (open symbols) for $\text{YMn}_{1-x}\text{Fe}_x\text{O}_3$ (all compositions) and under 5T-field (closed symbols) for the doped-specimens. Insets depict the variations of the cell-volume.

Fig.8. Temperature-dependence of the ordered magnetic moment μ_{ord} in zero-field (open symbols) for $\text{YMn}_{1-x}\text{Fe}_x\text{O}_3$ (all compositions), and under 5T-field (closed symbols) for the doped-specimens. Inset depicts (scaled to $\mu_{ord}(10\text{K})$ of the pure YMnO_3) zero-field μ_{ord} vs. the Fe-content at 10K, 30K, 50K, and 60K; evidencing nil contribution from the fully-fluctuating Fe-moments [$\mu_{ord}(x=0.1) \equiv 0.9\mu_{ord}(x=0)$], and smaller than maximum-expected values for the mixed-structured $\text{YMn}_{0.95}\text{Fe}_{0.05}\text{O}_3$ [$\mu_{ord} < \mu_{ord}^{max} \approx 0.95\mu_{ord}(T, x=0)$], due to the weakly-ordered Mn-moments trapped in the Γ_1 - Γ_2 interfacial domain walls.

Fig.9. Left y -axis: zero-field $\Phi(T)$ as average over abundance, of the angle (90° for Γ_1 and 0° for Γ_2) between Mn-moment and the a -axis, in the mixed-structured $\text{YMn}_{0.95}\text{Fe}_{0.05}\text{O}_3$. Right y -axis: consequent T -dependences of Γ_1 - and Γ_2 -fractions; the magnetic structure evolves from Γ_1 -rich (low- T) to Γ_2 -rich (near- T_N) configuration. Inset: left y -axis-- thermal-evolution of the gross-fraction of residual-fluctuating Mn-moments ($1-[\mu_{ord}(T, x=0.05)/\mu_{ord}^{full}(x=0.05)]$); right y -axis-- thermal-dissolution of estimated net-fraction of weakly-ordered Mn-moments trapped within the Γ_1 - Γ_2 domain walls ($1-[\mu_{ord}(T, x=0.05)/\mu_{ord}^{max}(T, x=0.05)]$).

Fig.1

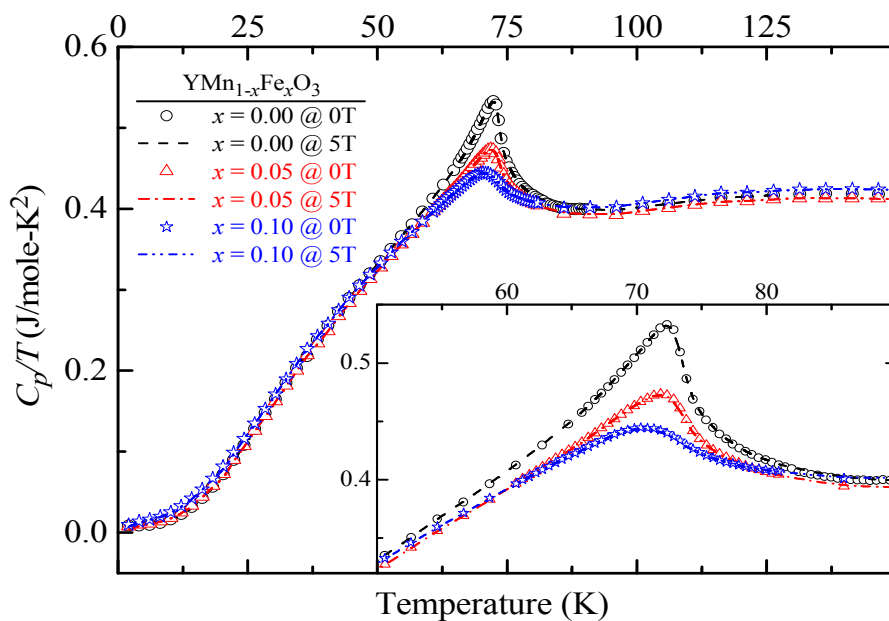


Fig.2

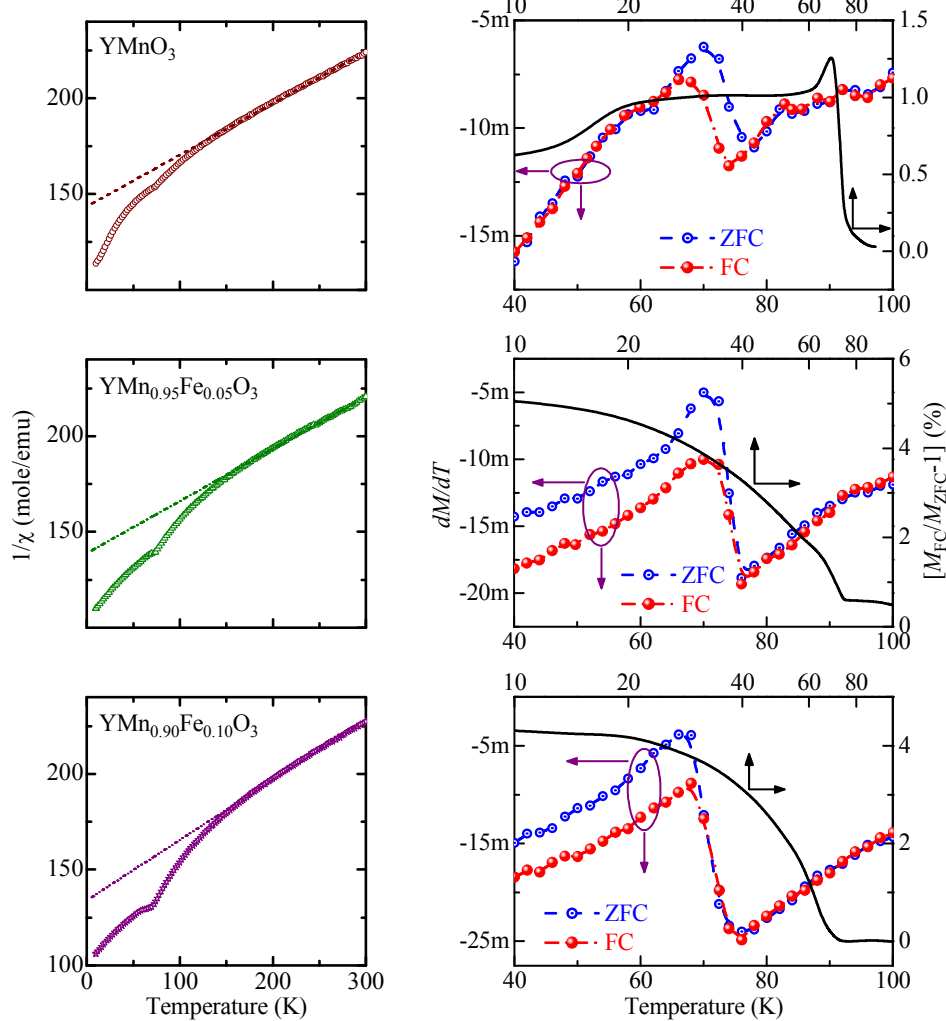


Fig.3

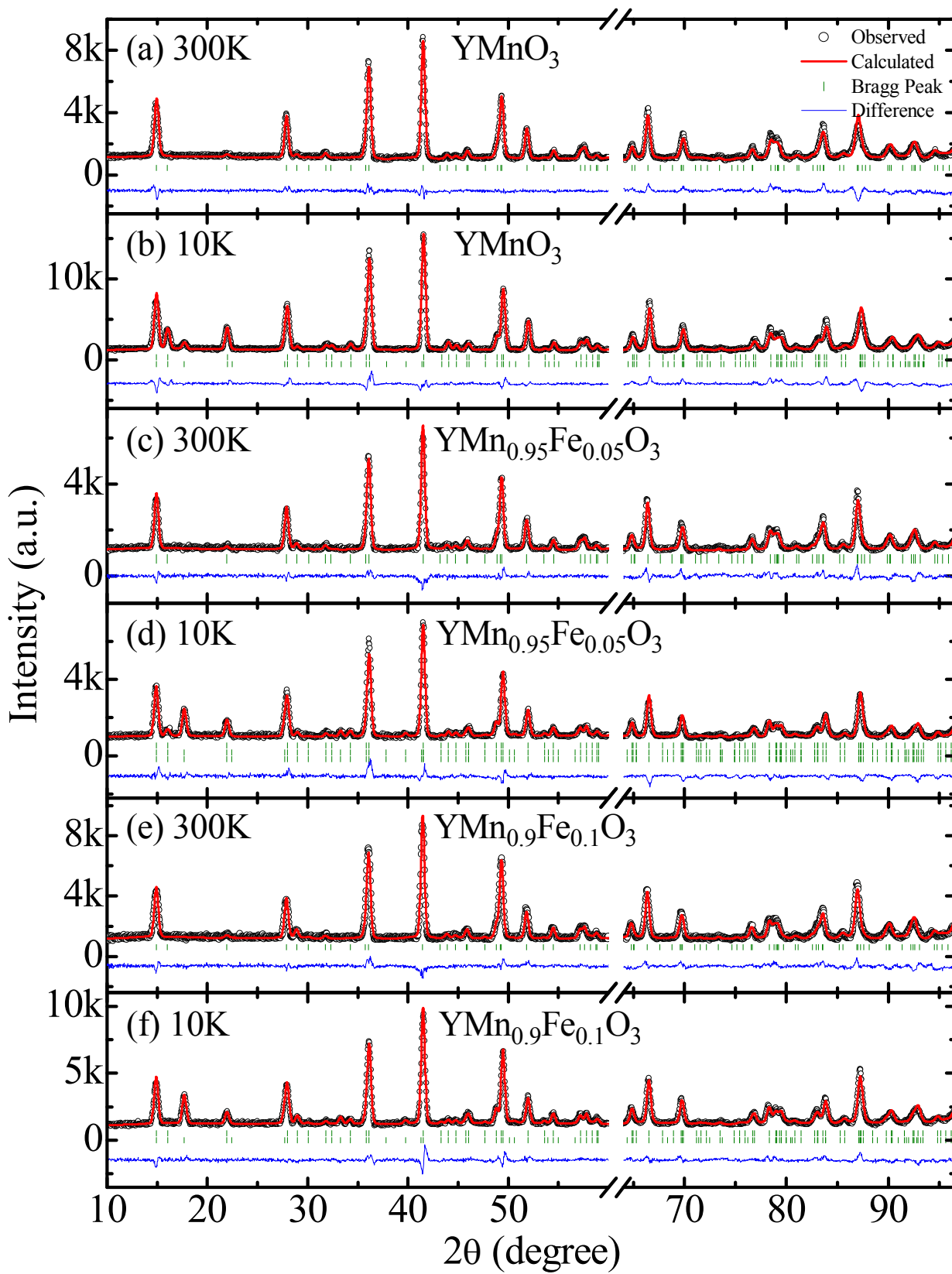


Fig.4

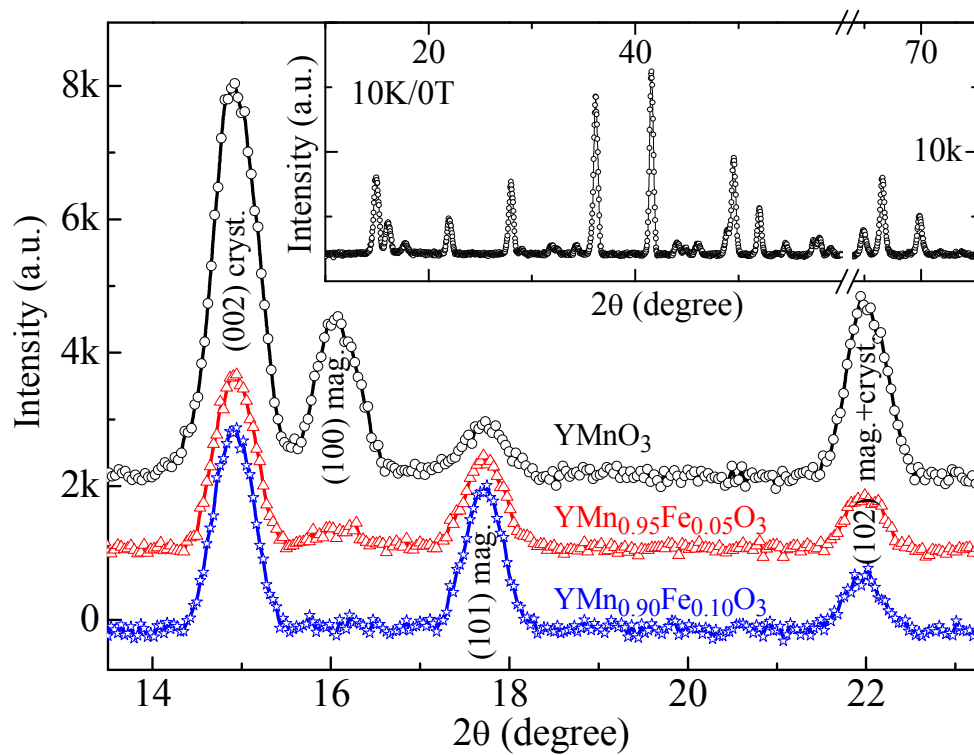


Fig.5

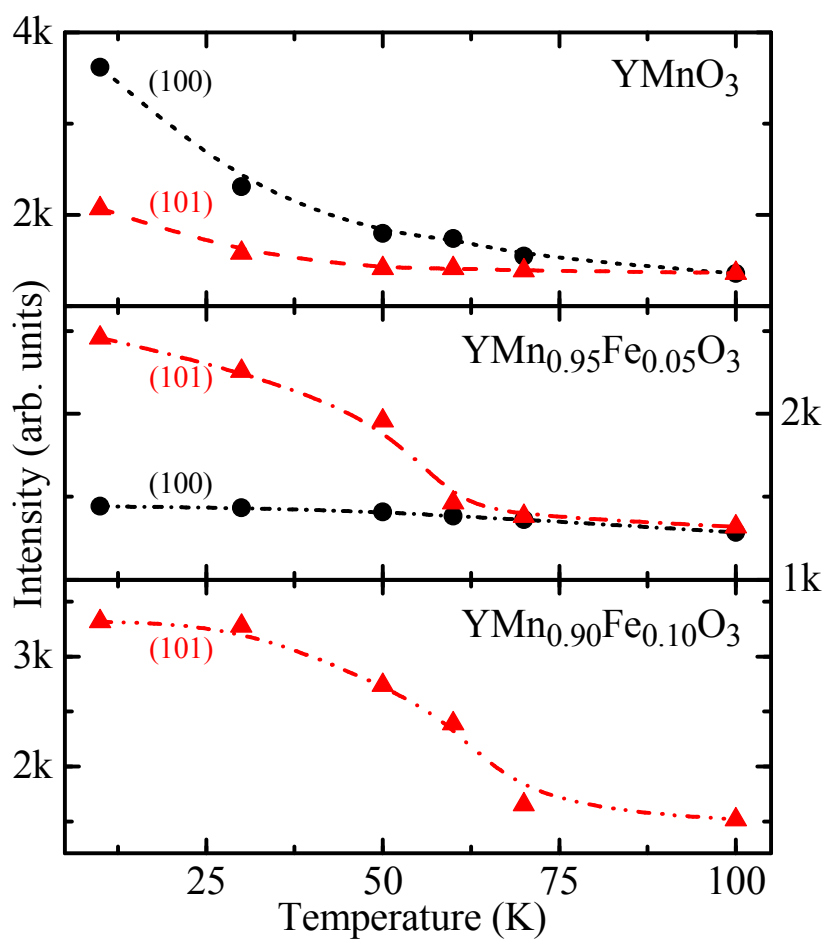


Fig.6

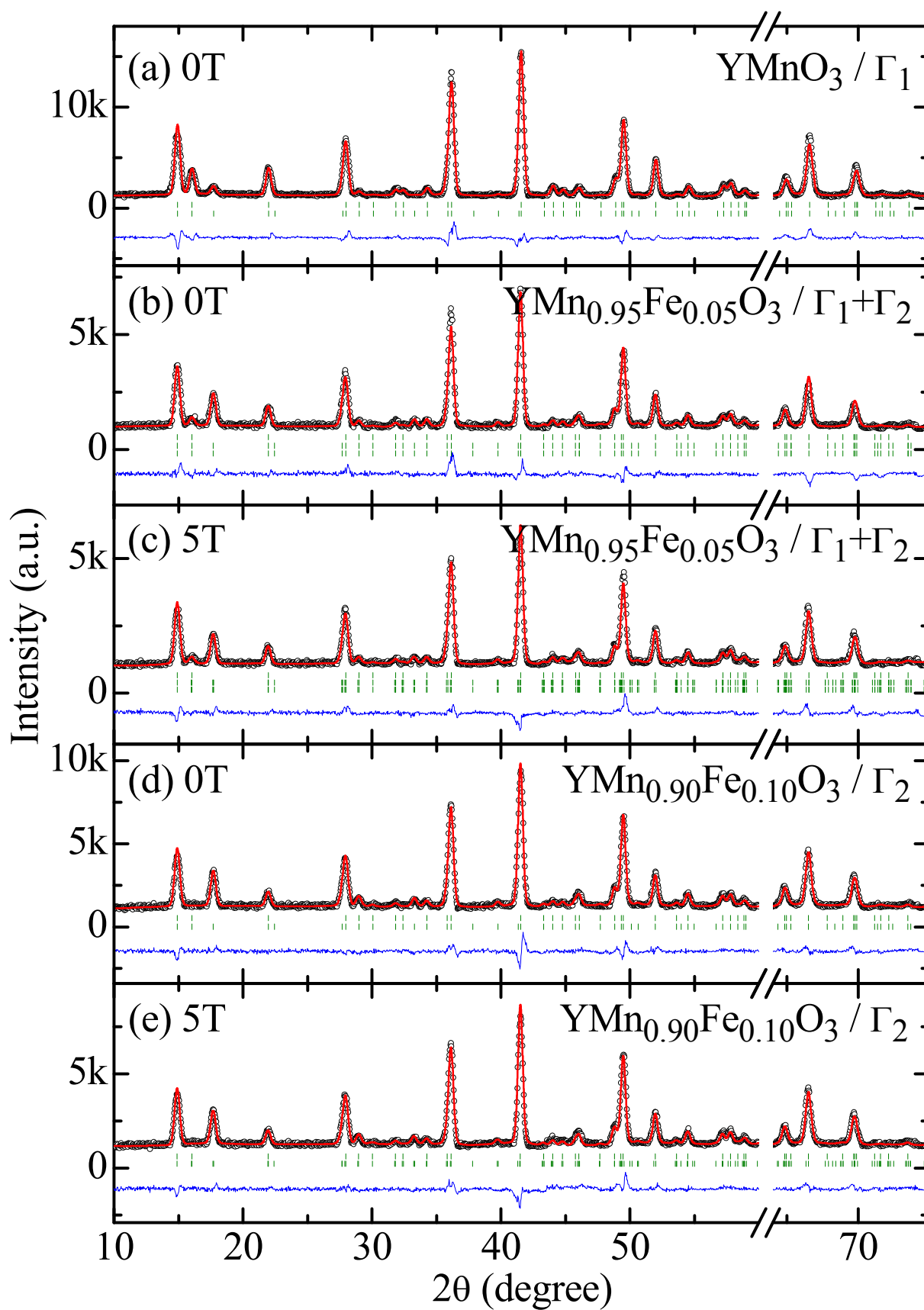


Fig.7

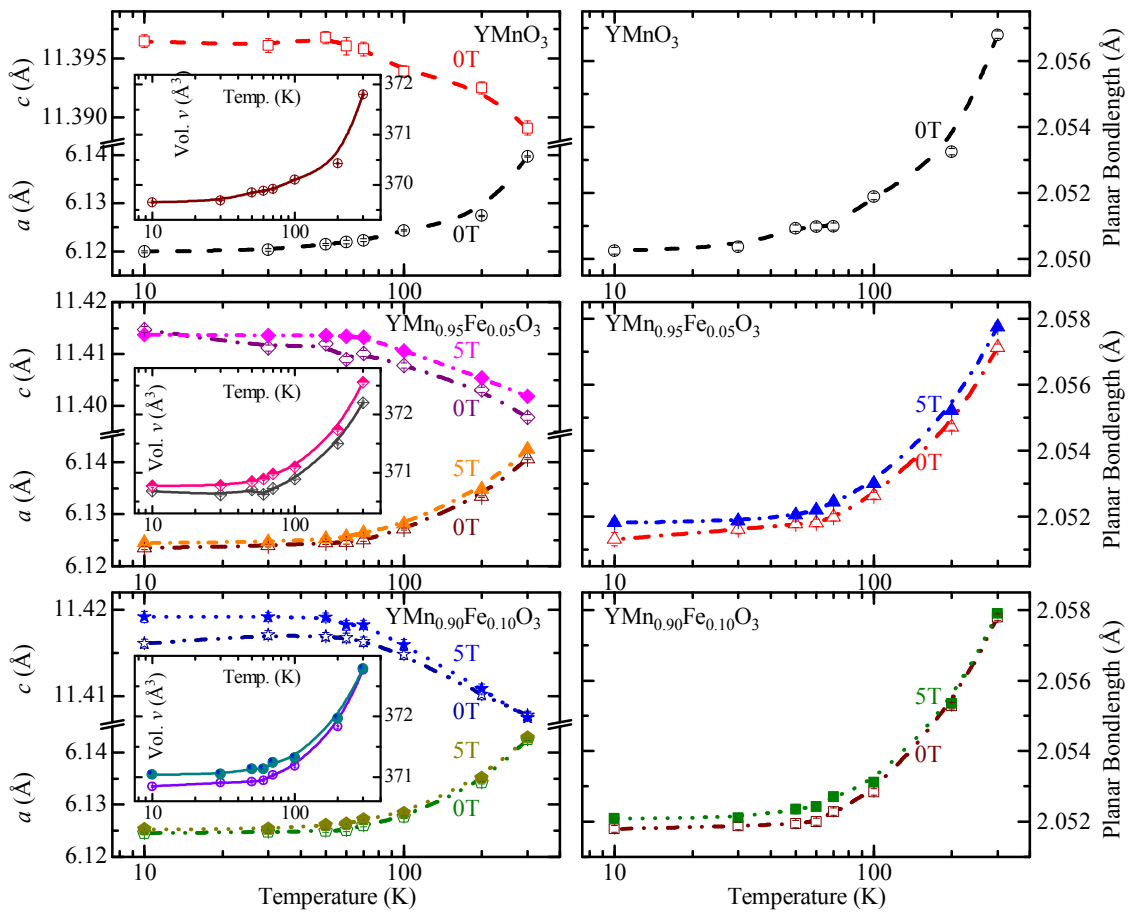


Fig.8

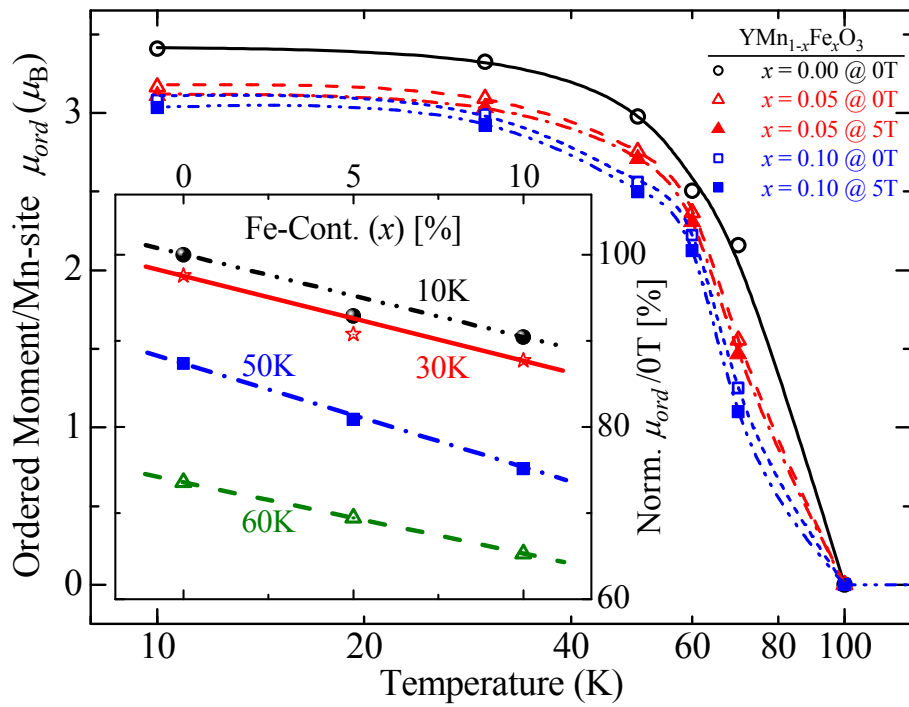


Fig.9

